Large-Signal Modeling of Grid-Following Inverter: from Sixth-Order Model to Second-Order Model

Huang, Liang; Wu, Chao; Zhou, Dao; Blaabjerg, Frede; He, Shan

Published in:
2024 IEEE 10th International Power Electronics and Motion Control Conference (IPEMC2024-ECCE Asia)

DOI (link to publication from Publisher):
10.1109/IPEMC-ECCEAsia60879.2024.10567659

Publication date:
2024

Document Version
Version created as part of publication process; publisher's layout; not normally made publicly available

Large-Signal Modeling of Grid-Following Inverter: from Sixth-Order Model to Second-Order Model

Liang Huang[1], Chao Wu[2], Dao Zhou[1], Frede Blaabjerg[1], and Shan He[3]
[1] Aalborg University, Denmark
[2] Shanghai Jiao Tong University, China
[3] Kiel University, Germany

***Abstract*--As penetration of wind power plants increases, the grid condition becomes increasingly weaker, which may make grid-following (GFL) inverters lose synchronization under large grid disturbances. In prior research, most researchers study transient stability of GFL inverters based on a simplified second-order model. Namely, the focus is solely on dynamics of phase-locked loop. However, this simplified second-order model may lose partial accuracy. Moreover, the reasonability of the simplification has not been clearly clarified. To fill this research gap, this paper provides a deduction process from an accurate high-order model to several reduced-order models. It is found that when the dynamics of filter capacitors are ignored, the accuracy of the model is still high. However, neglecting current control loops and the dynamics of grid inductors will moderately decrease the accuracy of the model. Finally, time-domain simulations have confirmed the validity of the proposed several large signal models.**

***Index Terms*—large-signal model, grid-following inverter, weak grid condition, transient stability.**

I. INTRODUCTION

In response to the anticipated depletion of fossil fuels and concerns over global warming attributed to CO2 emissions, renewable energy power plants, including wind and solar installations, have seen widespread deployment globally [1]-[3]. Given that wind and solar power plants are interconnected with the power system via inverters, the stability of power system is contingent upon the stability of these grid-connected inverters [4]-[6]. Nevertheless, with the gradual weakening of the power grid, grid-connected inverters utilizing the standard grid-following (GFL) control may experience losing synchronization stability during severe faults [7]-[9]. Therefore, the modeling of grid-connected inverters under large-signal disturbances and the analysis of transient stability have attracted lots of research attention recently [10]-[13].

To study the transient stability issues, two aspects should be considered: the first aspect is whether the system has an equilibrium point in steady-state; The second aspect is whether the system can converge to the equilibrium point after a large disturbance [9]. The main mathematical challenge of analyzing transient stability is the second aspect. This is because as the order of the nonlinear differential equations increases, it becomes more difficult to find a mathematical solution. Due to this reason, in most existing research, the GFL inverter system is simplified to be a second-order large-signal model to study the transient stability, where only the phase-locked loop (PLL) dynamics are considered [14]-[16]. In addition, some recent studies reveal that the transient stability is impacted by the dynamics of the current control loop as well, so that a fourth-order large-signal model considering current control loop's dynamics is introduced accordingly [17], [18]. However, step-by-step model reduction and comparison of different models have not been studied thoroughly in the existing research.

To address this research deficiency, this paper focuses on step-by-step model reduction and the impact of relevant parameters on models and transient stability. Firstly, a GFL controlled current source (CCS) is chosen for study, where current control loop's dynamics are intentionally ignored. By using this GFL controlled CCS system, the influence of the current control loop's dynamics and other dynamics can be separated, which enables a simpler and more intuitive model representation. Secondly, a sixth-order large-signal model is derived, where dynamics of the filter capacitors, the grid inductors, and the PLL are included. Based on simulation analysis, it demonstrates that the proposed sixth-order model adequately captures the characteristics of the GFL CCS. Afterwards, the sixth-order model is condensed into a fourth-order model by neglecting the filter capacitors, and it is further condensed into a second-order model by neglecting dynamics of the grid inductors. By comparing these models, it is found that the dynamics of the filter capacitors are negligible. However, when the dynamics of the grid inductors are ignored, partial accuracy of the model may be lost. In addition, from the transient stability perspective, PLL is indeed a main reason for transient instability.

The remainder of this paper is structured as below. Section II introduces large-signal modeling process of grid-following inverters, where several reduced-order models are provided. Then, Section III presents the mathematical expressions of different reduced-order models. Afterward, Section IV introduces three study cases to illustrate which condition may lead to transient instability. Ultimately, Section V summarizes this paper.

II. MODELING FOR GRID-FOLLOWING INVERTERS

The physical setup of GFL inverter system is depicted in Fig. 1(a).

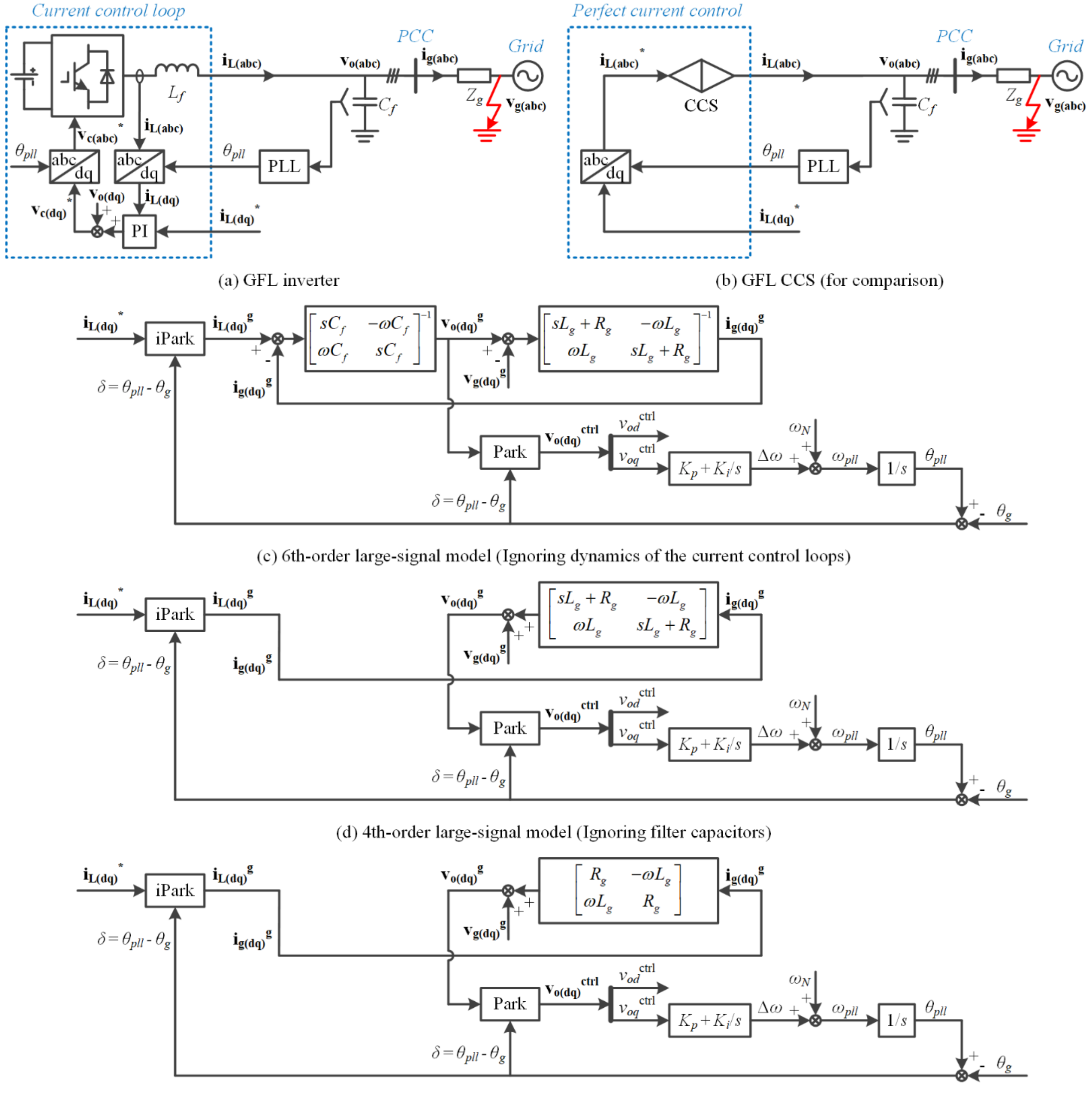

(a) GFL inverter
(b) GFL CCS (for comparison)
(c) 6th-order large-signal model (Ignoring dynamics of the current control loops)
(d) 4th-order large-signal model (Ignoring filter capacitors)
(e) 2nd-order large-signal model (Ignoring dynamics of the grid inductors)

Fig. 1. Large-signal models of grid-following inverter.

As depicted in Fig. 1(a), the study system consists of a GFL inverter and a Thevenin equivalent grid. The inverter and the grid connect at the point of common coupling (PCC). Besides, the typical GFL control scheme with a PLL and current control loops is chosen for analysis in this paper, where the PLL structure is the same as [14] and [19]. For sake of simplification, the current control loop is replaced by an ideal CCS for comparison. Moreover, the block “iPark” in Fig. 1 means inverse Park transformation.

According to the GFL CCS depicted in Fig. 1(b), a 6th-order large-signal model in the d-q frame is obtained, as depicted in Fig. 1(c). Notably, the superscript ‘g’ denotes the grid d-q frame, while the superscript ‘ctrl’ represents the control d-q frame. Then, when the filter capacitors are ignored, the 6th-order large-signal model can be simplified to be a 4th-order large-signal model, as depicted in Fig. 1(d). Furthermore, while dynamics of the grid inductors are ignored, the 4th-order large-signal model is able to be simplified to be a 2nd-order model, as shown in Fig. 1(e), where only the PLL dynamics are included. In fact, it is equivalent to the 2nd-order model proposed in [14] (See Fig. 9). Moreover, the models shown in Fig. 1 can also be represented by equations. The equation of v_{oq}^{ctrl} is a key equation, which is presented in (1).

$$v_{oq}^{\ ctrl} = -\sin(\delta)\cdot v_{od}^{\ g} + \cos(\delta)\cdot v_{oq}^{\ g} \tag{1}$$

Here, δ represents angle difference between θ_{pll} and θ_g.

Notably, when choosing different large-signal models, the variables v_{od}^{g} and v_{oq}^{g} in (1) are different, which leads to a different v_{oq}^{ctrl}.

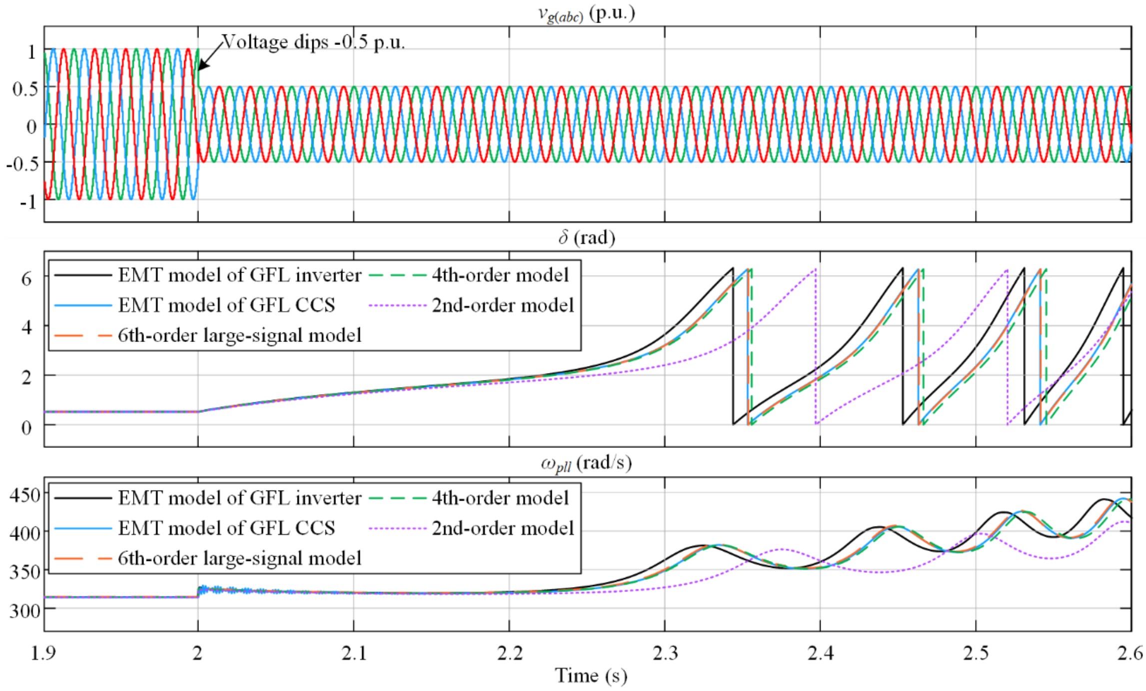

Fig. 2. Comparison of different models by time-domain simulation (Grid condition: SCR = 1 and R_g/X_g = 0.1).

To compare different models, simulation results for these models are depicted in Fig. 2 (See Table I for parameters). Notably, an inductance-dominated weak grid condition with a short-circuit ratio (SCR) = 1 and R_g/X_g = 0.1 is selected. It shows that under grid voltage dip conditions, responses of the 6th-order and 4th-order models are close to responses of the GFL CCS, while responses of the 2nd-order model are different. It means that the 2nd-order model is less accurate than the 6th-order and 4th-order models. In accordance with the above analysis, the 4th-order model could be a good choice for large-signal modeling and transient stability analysis, because it is relatively simple and accurate.

In addition, the differences between the simulation outcomes of GFL inverters and GFL CCS can be observed in Fig. 2, which is because of neglection of inner current loop's dynamics. However, the impact of the inner current loop on large-signal models and large-signal transient stability falls beyond this paper's scope, which will be explored in future research.

III. Mathematical Expressions of Reduced-Order Large-Signal Models

In the last section, the analysis is mainly based on the block diagram of models in MATLAB/Simulink shown in Fig. 1, which is relatively time-consuming. A more efficient way is using a solver to solve mathematical expressions, and it will be elaborated as follows.

A. Sixth-Order Large-Signal Model

At first, in accordance with Fig. 1(c), dynamics of the PLL is able to be derived as (2) and (3).

$$\dot{\delta} = \Delta\omega + \omega_N - \omega_g \tag{2}$$

$$\Delta\dot{\omega} = K_p \cdot \dot{v}_{oq}^{\mathrm{ctrl}} + K_i \cdot v_{oq}^{\mathrm{ctrl}} \tag{3}$$

Besides, the grid impedance's dynamics can be represented by (4).

$$\begin{cases} L_g \dot{i}_{gd}{}^{g} + R_g i_{gd}{}^{g} - \omega_N L_g i_{gq}{}^{g} = v_{od}{}^{g} - v_{gd}{}^{g} \\ \omega_N L_g i_{gd}{}^{g} + L_g \dot{i}_{gq}{}^{g} + R_g i_{gq}{}^{g} = v_{oq}{}^{g} - v_{gq}{}^{g} \end{cases} \tag{4}$$

Moreover, the dynamics of the capacitor is given by (5).

$$\begin{cases} C_f \dot{v}_{od}{}^{g} - \omega_N C_f v_{oq}{}^{g} = i_{Ld}{}^{g} - i_{gd}{}^{g} \\ \omega_N C_f v_{od}{}^{g} + C_f \dot{v}_{oq}{}^{g} = i_{Lq}{}^{g} - i_{gq}{}^{g} \end{cases} \tag{5}$$

Furthermore, the inverse Park transformation of the currents can be derived as (6).

$$\begin{cases} i_{Ld}{}^{g} = \cos(\delta) \cdot i_{Ld}{}^{*} - \sin(\delta) \cdot i_{Lq}{}^{*} \\ i_{Lq}{}^{g} = \sin(\delta) \cdot i_{Ld}{}^{*} + \cos(\delta) \cdot i_{Lq}{}^{*} \end{cases} \tag{6}$$

Then, the 6th-order large-signal model can be obtained by combining equations (1)-(6), where the state variables are [δ, $\Delta\omega$, $v_{od}{}^{g}$, $v_{oq}{}^{g}$, $i_{gd}{}^{g}$, $i_{gq}{}^{g}$]. More comprehensive expressions of the 6th-order model are presented in (A1) located in Appendix.

B. Fourth-Order Large-Signal Model (C_f = 0)

It depicts in Fig. 1(d) that while filter capacitor is assumed equal to 0, (5) can be simplified as (7).

$$\begin{cases} i_{Ld}{}^{g} = i_{gd}{}^{g} \\ i_{Lq}{}^{g} = i_{gq}{}^{g} \end{cases} \tag{7}$$

Then, the 4th-order large-signal model can be derived by combining the equations (1)-(4), (6), and (7), which is given by (8). The state variables are [δ, $\Delta\omega$, $i_{gd}{}^{g}$, $i_{gq}{}^{g}$].

$$
\begin{cases}
\dot{\delta} = \Delta\omega + \omega_N - \omega_g \\
\Delta\dot{\omega} = K_p \cdot [-\sin(\delta)\dot{v}_{od}{}^{g} - \cos(\delta)\dot{\delta}\cdot v_{od}{}^{g} + \cos(\delta)\dot{v}_{oq}{}^{g} \\
-\sin(\delta)\dot{\delta}\cdot v_{oq}{}^{g}] + K_i \cdot [-\sin(\delta) v_{od}{}^{g} + \cos(\delta) v_{oq}{}^{g}] \\
\dot{i}_{gd}{}^{g} = \dfrac{1}{L_g}(v_{od}{}^{g} - v_{gd}{}^{g} + \omega_N L_g i_{gq}{}^{g} - R_g i_{gd}{}^{g}) \\
\dot{i}_{gq}{}^{g} = \dfrac{1}{L_g}(v_{oq}{}^{g} - v_{gq}{}^{g} - \omega_N L_g i_{gd}{}^{g} - R_g i_{gq}{}^{g}) \\
i_{gd}{}^{g} = i_{Ld}{}^{g} = \cos(\delta)\cdot i_{Ld}{}^{*} - \sin(\delta)\cdot i_{Lq}{}^{*} \\
i_{gq}{}^{g} = i_{Lq}{}^{g} = \sin(\delta)\cdot i_{Ld}{}^{*} + \cos(\delta)\cdot i_{Lq}{}^{*}
\end{cases} \tag{8}
$$

When the variables $i_{Ld}{}^{*}$, $i_{Lq}{}^{*}$, $v_{gd}{}^{g}$, $v_{gq}{}^{g}$ and ω_g are assumed to be constant, (8) is simplified to be (9).

$$
\begin{cases}
\dot{\delta} = \Delta\omega \\
\Delta\dot{\omega} = \dfrac{-K_p}{1 - K_p L_g i_{Ld}{}^{*}} \cdot \cos(\delta)\cdot V_g \cdot \Delta\omega + \\
\dfrac{K_i}{1 - K_p L_g i_{Ld}{}^{*}} \cdot [(\Delta\omega + \omega_N) L_g i_{Ld}{}^{*} + R_g i_{Lq}{}^{*} - \sin(\delta)\cdot V_g]
\end{cases} \tag{9}
$$

Thus, transient stability analysis can be performed by phase portrait according to (9).

C. *Second-Order Large-Signal Model ($sL_g = 0$)*

It shows in Fig. 1(e) that while the grid inductors' dynamics are ignored, (4) can be rewritten as (10).

$$
\begin{cases}
R_g i_{gd}{}^{g} - \omega_N L_g i_{gq}{}^{g} = v_{od}{}^{g} - v_{gd}{}^{g} \\
\omega_N L_g i_{gd}{}^{g} + R_g i_{gq}{}^{g} = v_{oq}{}^{g} - v_{gq}{}^{g}
\end{cases} \tag{10}
$$

Then, the 2nd-order large-signal model can be deducted by combining the equations (1)-(3), (6), (7), and (10), which is presented by (11).

$$
\begin{cases}
\dot{\delta} = \Delta\omega + \omega_N - \omega_g \\
\Delta\dot{\omega} = K_p \cdot [-\dot{\delta}\cdot\cos(\delta)\cdot V_g] \\
+K_i \cdot [\omega_N L_g i_{Ld}{}^{*} + R_g i_{Lq}{}^{*} - \sin(\delta)\cdot V_g]
\end{cases} \tag{11}
$$

Obviously, the 2nd-order model is much simpler. According to (11), transient stability of GFL inverters is impacted by grid voltage magnitude V_g, grid inductance L_g, grid resistance R_g, and d-q currents $i_{Ld}{}^{*}$ and $i_{Lq}{}^{*}$. So, the impact of the three factors on transient stability will be analyzed in the following section.

IV. Transient Stability Analysis of Three Cases

Considering transient stability of GFL inverters may be influenced by several factors, such as V_g, L_g, R_g, $i_{Ld}{}^{*}$ and $i_{Lq}{}^{*}$, three cases are selected in this paper for study, as presented in Table I. Specifically, in the selected three cases, the impact of q-axis and d-axis currents, the impact of the depth of grid voltage dip, and the impact of the grid impedance's R/X ratio are analyzed quantitatively.

TABLE I
PARAMETERS OF SELECTED STUDY CASES

General Parameters	Nominal power of inverter	30 kW
	Rated line voltage (RMS)	380 V
	Nominal grid frequency	50 Hz
	Filter inductance, capacitance	0.15 p.u. and 0.02 p.u.
	SCR and R_g/X_g	1 and 0.1
	Bandwidth of current loop	6000 rad/s
	ξ and ω_n of the PLL	1 and 20 rad/s
Case 1	(a) $i_{Ld}{}^{*}$ = 0.5 p.u., $i_{Lq}{}^{*}$ = 0; (b) $i_{Ld}{}^{*}$ = 0, $i_{Lq}{}^{*}$ = -0.5 p.u.	
Case 2	(a) R_g/X_g = 0.3; (b) R_g/X_g = 0.1 Note: $i_{Ld}{}^{*}$ = 0, $i_{Lq}{}^{*}$ = -0.8 p.u. for both (a) and (b)	
Case 3	(a) V_{g_fault} = 0.1 p.u.; (b) V_{g_fault} = 0.2 p.u. Note: $i_{Ld}{}^{*}$ = 0, $i_{Lq}{}^{*}$ = -0.9 p.u. for both (a) and (b)	

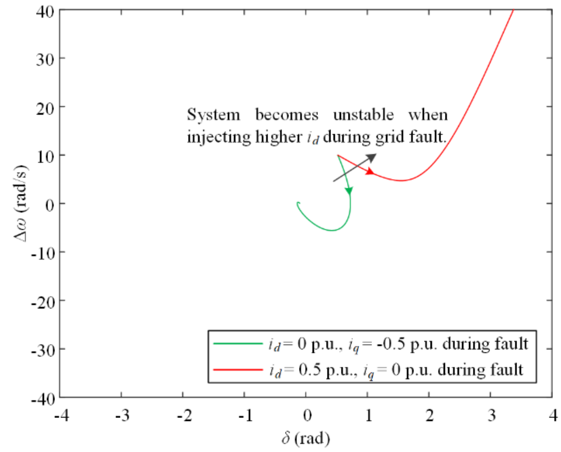

Fig. 3. Phase portrait of Case 1.

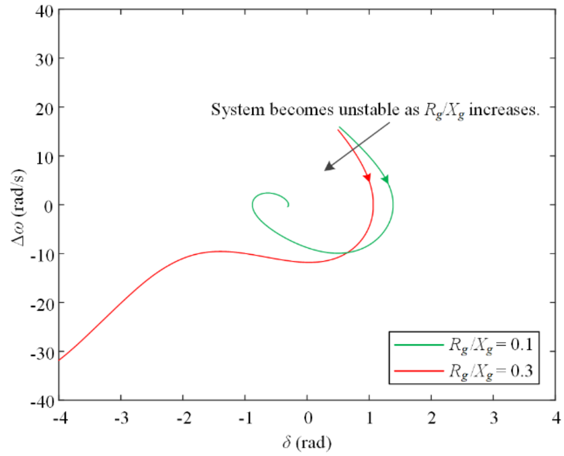

Fig. 4. Phase portrait of Case 2.

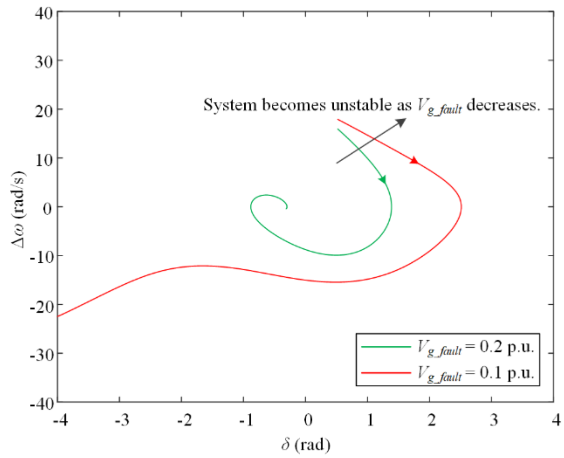

Fig. 5. Phase portrait of Case 3.

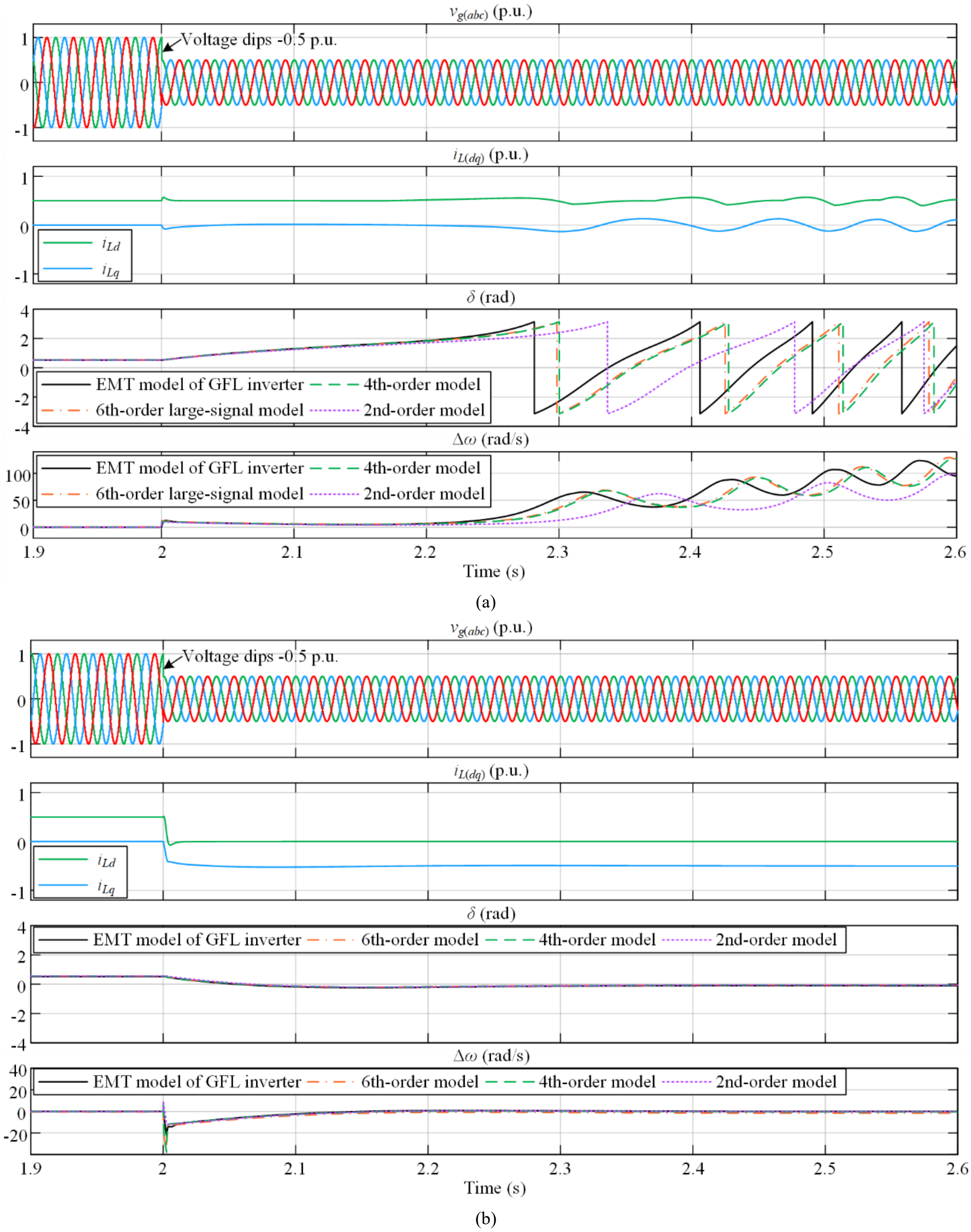

Fig. 6. Simulation outcomes of Study Case 1. (a) $i_{Ld} = 0.5$ p.u., $i_{Lq} = 0$; (b) $i_{Ld} = 0$, $i_{Lq} = -0.5$ p.u.

A. Study Case 1: Impact of q-axis and d-axis currents

According to (9) and (11), the current i_{Lq} and the current i_{Ld} influence transient stability. So, for the first study case, i_{Ld} and i_{Lq} are chosen to be different values, as presented in Table I. The phase portrait of Study Case 1 is depicted in Fig. 3, which shows that a higher i_{Ld} during grid fault may lead to instability.

B. Study Case 2: Impact of R/X ratio of grid impedance

Besides, according to (9) and (11), the grid resistance R_g and the inductance L_g also influence transient stability. So, for the second study case, R_g/X_g is given by different values, as presented in Table I. The phase portrait of Study Case 2 is depicted in Fig. 4, which shows that a higher R_g/X_g during grid fault may cause instability.

C. Study Case 3: Impact of the depth of grid voltage dip

Moreover, according to (9) and (11), the depth of grid voltage dip has also an impact on transient stability. So, for the third study case, V_{g_fault} is given by different values for comparison, as presented in Table I. The phase portrait of Study Case 3 is given in Fig. 5, which shows that a deeper grid voltage dip may lead to instability.

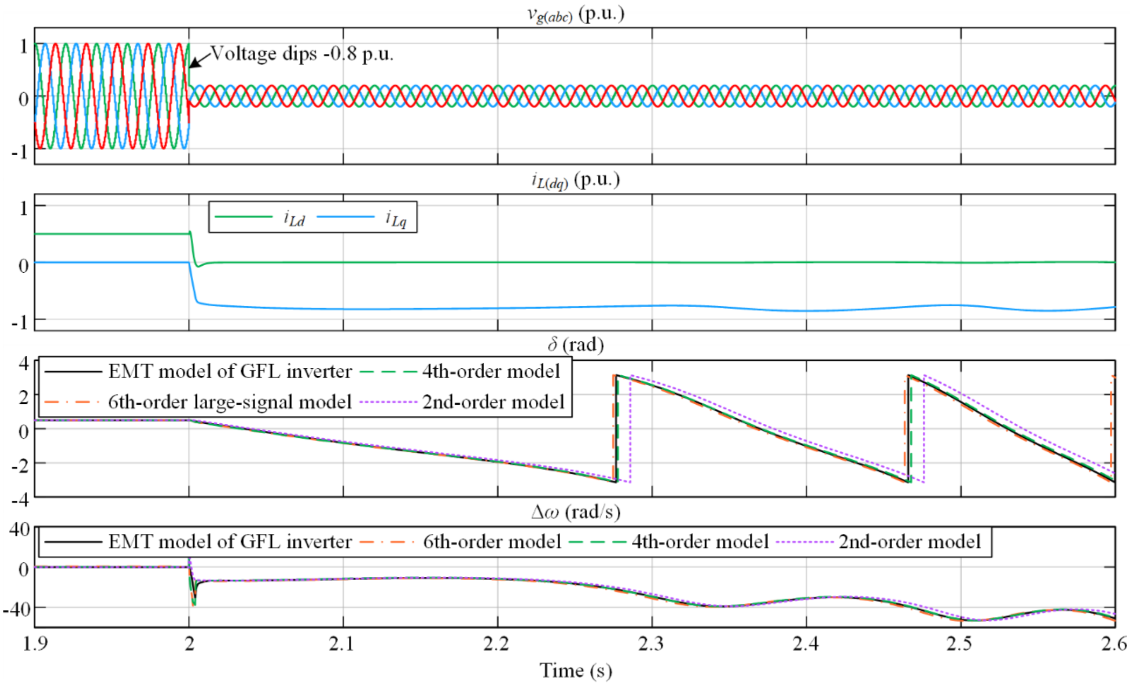

(a)

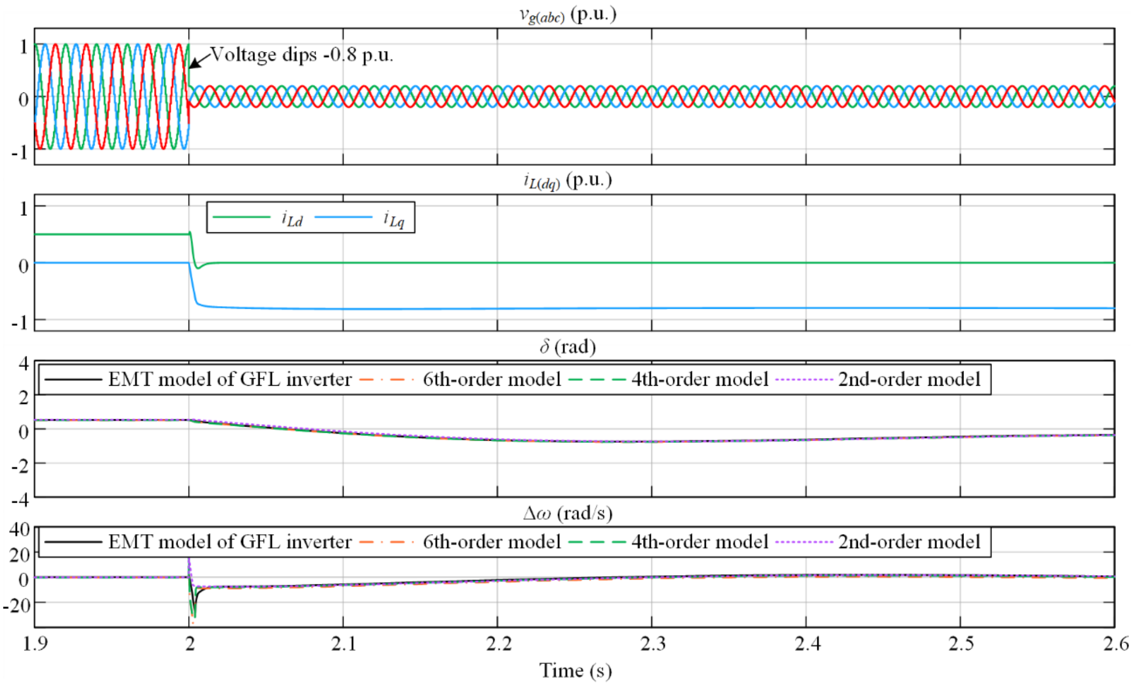

(b)

Fig. 7. Simulation outcomes of Study Case 2. (a) $R_g/X_g = 0.3$; (b) $R_g/X_g = 0.1$.

To validate the transient stability analysis results in Figs. 3-5, simulation outcomes of these selected three study cases are presented in Figs. 6-8.

As depicted in Fig. 6(a), while current i_{Ld} is 0.5 p.u., the system becomes unstable during grid fault. However, while the current i_{Ld} is decreased to 0 during grid fault, the system is able to keep stable, as shown in Fig. 6(b). Hence, a smaller i_{Ld} during grid fault contributes positively to transient stability of GFL inverters. These simulation outcomes agree with the analysis results in Fig. 3.

In addition, as depicted in Fig. 7(a), while the ratio of R_g and X_g is 0.3, the system becomes unstable during grid fault. Nevertheless, as depicted in Fig. 7(b), while the ratio of R_g and X_g is 0.1, the system always keeps stable. Therefore, a larger grid resistance R_g is worse for transient stability of GFL inverters.

Furthermore, as depicted in Fig. 8(a), when the grid voltage dips -0.9 p.u., it becomes unstable during fault. However, as presented in Fig. 8(b), while grid voltage dips -0.8 p.u., it keeps stable during the fault. Thus, a lower grid voltage magnitude during the fault is worse for transient stability of GFL inverters.

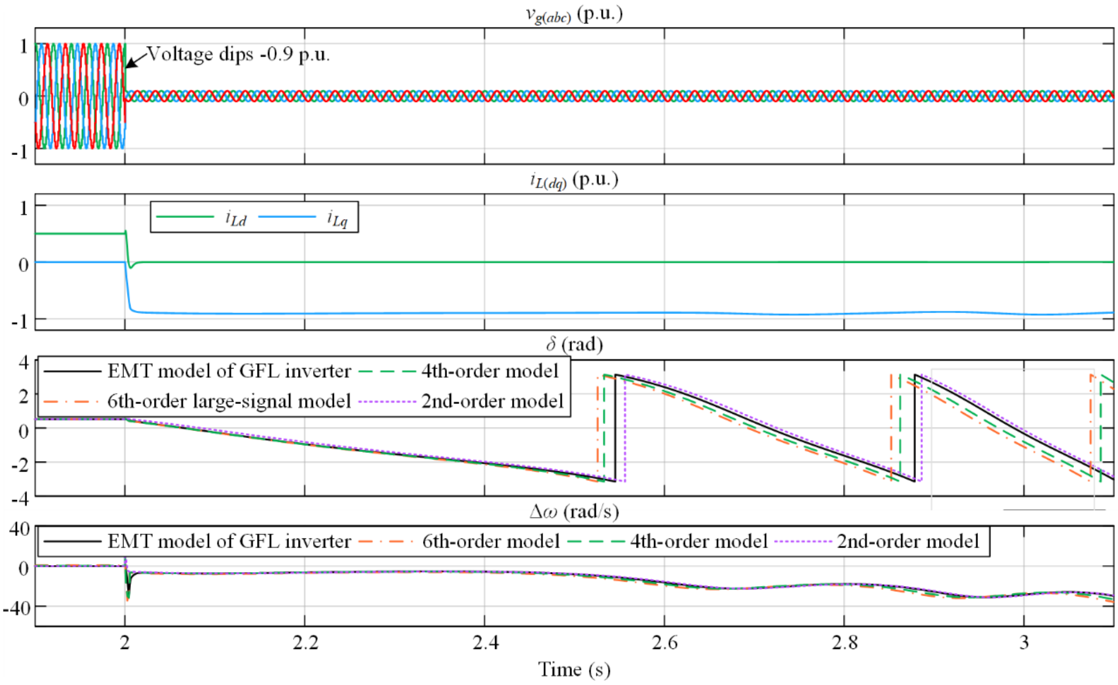

(a)

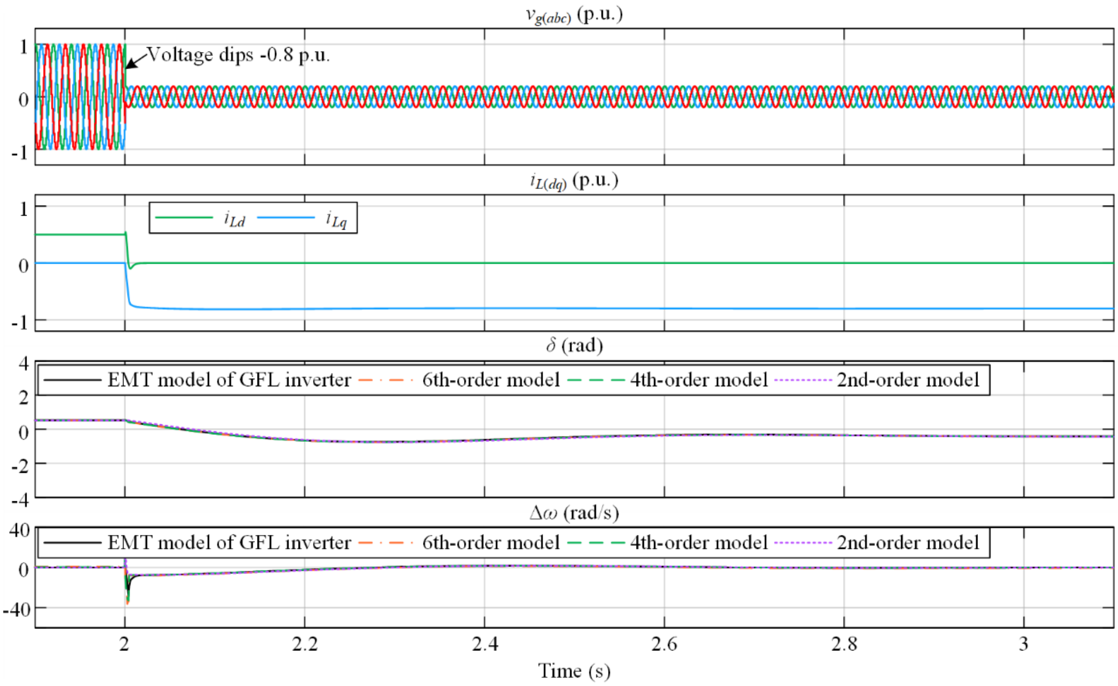

(b)

Fig. 8. Simulation outcomes of Study Case 3. (a) Grid voltage dips -0.9 p.u.; (b) Grid voltage dips -0.8 p.u.

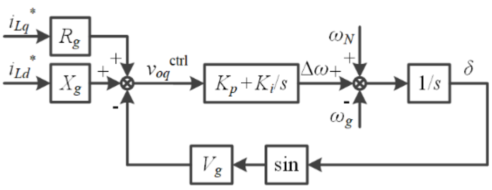

Fig. 9. Equivalent block diagram of Fig. 1(e).

Aside from the above analysis, it can also be seen from Figs. 6-8 that the 6th-order, 4th-order, and 2nd-order models all have the same trend of stability for the selected three study cases, which means that the transient instability issue of the GFL inverter should be mainly caused by the PLL. To understand the reason for transient instability issue, the 2nd-order model depicted in Fig. 1(e) is represented in a simpler form depicted in Fig. 9. It shows that if there is a way to keep "$v_{oq}^{ctrl} = 0$" (Namely, $R_g \cdot i_{Lq}^* + X_g \cdot i_{Ld}^* = V_g \cdot \sin\delta$) during grid fault, an equilibrium point always exists. Therefore, a possible solution is to keep "$i_{Ld}^* = -R_g/X_g \cdot i_{Lq}^*$" during grid fault [13]. Another simpler way is to keep both i_{Ld}^* and i_{Lq}^* equal to 0 during grid fault. However, they conflict with existing grid codes, but it may bring new thoughts to modify grid codes in the future.

V. Conclusions

Three reduced-order large-signal models of GFL inverters are compared in this paper.The 6th-order model and the 4th-order model have higher accuracy than the 2nd-order model. Namely, the filter capacitors' dynamics may be negligible, but when the dynamics of grid inductors are ignored, the accuracy of the model will be reduced moderately. Moreover, in accordance with stability analysis results of the selected three cases, it is revealed that a higher d-axis current, a higher grid impedance R/X ratio, and a deeper voltage dip during grid faults may cause transient instability of GFL inverters. Finally, a simple solution to keep "$i_{Ld}^* = 0$ and $i_{Lq}^* = 0$" during faults is proposed to raise transient stability, but it conflicts with existing grid codes. A more sensible control solution will be studied in the future.

Appendix

$$\begin{cases} \dot{\delta} = \Delta\omega + \omega_N - \omega_g \\ \Delta\dot{\omega} = K_p \cdot [-\sin(\delta)\dot{v}_{od}{}^{g} - \cos(\delta)\dot{\delta}\cdot v_{od}{}^{g} + \cos(\delta)\dot{v}_{oq}{}^{g} \\ -\sin(\delta)\dot{\delta}\cdot v_{oq}{}^{g}] + K_i \cdot [-\sin(\delta)v_{od}{}^{g} + \cos(\delta)v_{oq}{}^{g}] \\ \dot{v}_{od}{}^{g} = \dfrac{1}{C_f}(i_{Ld}{}^{g} - i_{gd}{}^{g} + \omega_N C_f v_{oq}{}^{g}) \\ \dot{v}_{oq}{}^{g} = \dfrac{1}{C_f}(i_{Lq}{}^{g} - i_{gq}{}^{g} - \omega_N C_f v_{od}{}^{g}) \\ \dot{i}_{gd}{}^{g} = \dfrac{1}{L_g}(v_{od}{}^{g} - v_{gd}{}^{g} + \omega_N L_g i_{gq}{}^{g} - R_g i_{gd}{}^{g}) \\ \dot{i}_{gq}{}^{g} = \dfrac{1}{L_g}(v_{oq}{}^{g} - v_{gq}{}^{g} - \omega_N L_g i_{gd}{}^{g} - R_g i_{gq}{}^{g}) \\ i_{Ld}{}^{g} = \cos(\delta)\cdot i_{Ld}{}^{*} - \sin(\delta)\cdot i_{Lq}{}^{*} \\ i_{Lq}{}^{g} = \sin(\delta)\cdot i_{Ld}{}^{*} + \cos(\delta)\cdot i_{Lq}{}^{*} \end{cases} \quad \text{(A1)}$$

Acknowledgment

This work is supported by the Offshore Energy Hubs project funded by EUDP. The author would like to thank project partners D. Pagnani (Ørsted), D. Müller (DTU), and P. Mahat (Siemens Gamesa) for fruitful discussion.

References

[1] "Net Zero by 2050 - A Roadmap for the Global Energy Sector," International Energy Agency, Tech. Rep., 2021.

[2] "Getting fit for 55 and set for 2050," European Technology & Innovation Platform on Wind Energy, Tech. Rep., 2021.

[3] Y. Cheng *et al*, "Real-world subsynchronous oscillation events in power grids with high penetrations of inverter-based resources," *IEEE Trans. Power Syst.*, vol. 38, no. 1, pp. 316–330, Jan. 2023.

[4] N. Hatziargyriou *et al.*, "Definition and classification of power system stability – revisited & extended," *IEEE Trans. Power Syst.*, vol. 36, no. 4, pp. 3271–3281, Jul. 2021.

[5] X. Wang, M. G. Taul, H. Wu, Y. Liao, F. Blaabjerg, and L. Harnefors, "Grid-synchronization stability of converter-based resources – an overview," *IEEE Open J. Ind. Applicat.*, vol. 1, pp. 115–134, 2020.

[6] M. Schweizer, S. Almér, S. Pettersson, A. Merkert, V. Bergemann and L. Harnefors, "Grid-forming vector current control," *IEEE Trans. Power Electron.*, vol. 37, no. 11, pp. 13091-13106, Nov. 2022.

[7] M. K. Bakhshizadeh, S. Ghosh, G. Yang and Ł. Kocewiak, "Transient stability analysis of grid-connected converters in wind turbine systems based on linear Lyapunov function and reverse-time trajectory," *J Modern Power Syst. Clean Energy*, 2023, (Eary Access).

[8] X. Li *et al.*, "The largest estimated domain of attraction and its applications for transient stability analysis of PLL synchronization in weak-grid-connected VSCs," *IEEE Trans. Power Syst.*, vol. 38, no. 5, pp. 4107–4121, Sep. 2023.

[9] M. G. Taul, C. Wu, S.-F. Chou, and F. Blaabjerg, "Optimal controller design for transient stability enhancement of grid-following converters under weak-grid conditions," *IEEE Trans. Power Electron.*, vol. 36, no. 9, pp. 10251–10264, Sep. 2021.

[10] D. Pal, B. K. Panigrahi, B. Johnson, D. Venkatramanan, and S. Dhople, "Large-signal stability analysis of three-phase grid-following inverters," *IEEE Trans. Energy Convers.*, 2023, (Early Access).

[11] M. G. Taul, X. Wang, P. Davari, and F. Blaabjerg, "An overview of assessment methods for synchronization stability of grid-connected converters under severe symmetrical grid faults," *IEEE Trans. Power Electron.*, vol. 34, no. 10, pp. 9655–9670, Oct. 2019.

[12] M. G. Taul, X. Wang, P. Davari, and F. Blaabjerg, "An efficient reduced-order model for studying synchronization stability of grid-following converters during grid faults," in *2019 20th Workshop on Control and Modeling for Power Electronics (COMPEL)*, Toronto, ON, Canada: IEEE, Jun. 2019, pp. 1–7.

[13] Ö. Göksu, R. Teodorescu, C. L. Bak, F. Iov and P. C. Kjær, "Instability of Wind Turbine Converters During Current Injection to Low Voltage Grid Faults and PLL Frequency Based Stability Solution," *IEEE Trans. Power Syst.*, vol. 29, no. 4, pp. 1683-1691, July 2014.

[14] H. Wu and X. Wang, "An adaptive phase-locked loop for the transient stability enhancement of grid-connected voltage source converters," in *2018 IEEE Energy Conversion Congress and Exposition (ECCE)*, Portland, OR, USA: IEEE, Sep. 2018, pp. 5892–5898.

[15] X. Wang, H. Wu, X. Wang, L. Dall, and J. B. Kwon, "Transient stability analysis of grid-following VSCs considering voltage-dependent current injection during fault ride-through," *IEEE Trans. Energy Convers.*, vol. 37, no. 4, pp. 2749–2760, Dec. 2022.

[16] C. Wu, X. Xiong, M. Taul, and F. Blaabjerg, "On the equilibrium points in three-phase PLL based on the *d* -axis voltage normalization," *IEEE Trans. Power Electron.*, vol. 36, no. 11, pp. 12146–12150, Nov. 2021.

[17] C. Wu, Y. Lyu, Y. Wang, and F. Blaabjerg, "Transient synchronization stability analysis of grid-following converter considering the coupling effect of current loop and phase locked loop," *IEEE Trans. Energy Convers.*, pp. 1–10, 2023.

[18] J. Chen, M. Liu, T. O'Donnell, and F. Milano, "Impact of current transients on the synchronization stability assessment of grid-feeding converters," *IEEE Trans. Power Syst.*, vol. 35, no. 5, pp. 4131–4134, Sep. 2020.

[19] L. Huang, C. Wu, D. Zhou and F. Blaabjerg, "A double-PLLs-based impedance reshaping method for extending stability range of grid-following inverter under weak grid," *IEEE Trans. Power Electron.*, vol. 37, no. 4, pp. 4091-4104, April 2022.